A New Recognition Approach Based on Genetic Algorithm for Classifying Textures in Satellite SAR Images

Gholamreza Akbarizadeh

Electrical Engineering Department, Engineering Faculty, Shahid Chamran University of Ahvaz (SCU), Ahvaz 61357-831351, Iran

g.akbari@scu.ac.ir

Abstract

Image segmentation is an important step in texture recognition of Satellite Synthetic Aperture Radar (SAR) images. In this paper, an efficient method for texture recognition of SAR images is proposed based on extraordinary result of wavelet transform on texture feature extraction and the benefits of genetic algorithm (GA) as a classifier. First, texture feature is extracted by wavelet transform. Second, a feature vector composed of wavelet energy feature, kurtosis value of wavelet energy feature and gray values of eight-neighborhood of SAR image is formed. Then, segmentation of different textures is applied by using feature vector and level set function. Finally, the values of feature vector are used for training the classifier. Two different classes of datasets are used to show the experimental results. One is a simulated SAR image and the other is a real satellite SAR image. The results of experiments show the powerful ability of this algorithm to recognize different textures in Satellite SAR images.

Keywords

Synthetic Aperture Radar; Segmentation; Level Set; Active Contour; Fourth Order Cumulant; Genetic Algorithm (GA)

Introduction

Synthetic aperture radar (SAR) imaging has many applications for environmental monitoring, recognition, targeting, surveillance, earth-resource mapping, and military systems. SAR imaging has capabilities to provide broad-area imaging at high resolutions and to acquire images in inclement weather or during night as well as day. These applications are driven by the military's need for all-weather, day-and-night imaging sensors. Because of the ability to use in all weather conditions, day and night xerography time and the high spatial resolution, SAR imaging systems are known as the most popular remote sensing technique widely used in the past decades [1]. In [35], a portable chip based on SAR imaging system is designed which can be installed on SAR satellite and earth stations (terrain receivers) for transform the microwave signal to image as shown in Fig. 1. This Fig. describes how a Satellite SAR imaging system works.

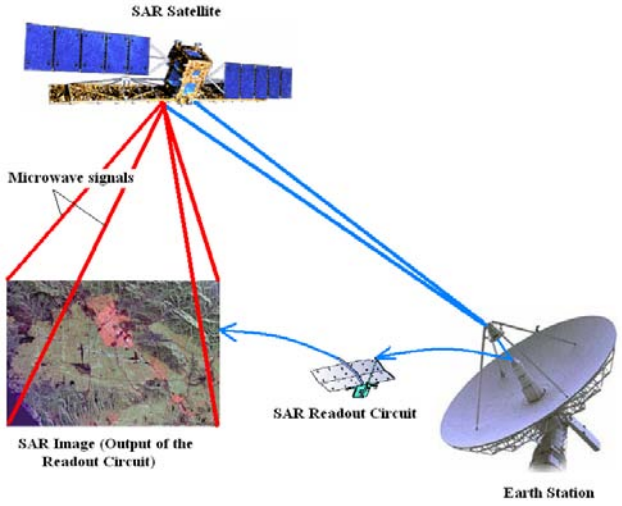

FIG. 1 THE CIRCUIT CHIP BASED ON SAR SATELLITE IMAGING SYSTEM PROPOSED IN [35]

In remote sensing applications, SAR imaging is a very powerful and attractive tool due to its high spatial resolution [2]. However, automatic interpretation of SAR images is extremely difficult because of the speckle noise [3]. The speckle noise is a perfectly expanded noise which SAR images are commonly modeled as influenced by it. SAR speckle can be described as multiplicative noise, with standard deviation equal to pixel reflectivity value [4]. The speckle noise also affects the probability density function (PDF) of the pixel intensities in SAR images. This phenomenon can be expressed by the nonlinear intensity inhomogeneity in SAR images [2]. This phenomenon causes that traditional image processing algorithms are not useful to SAR image processing. As

a result of this phenomenon, accurate segmentation for SAR images is still a crucial issue. So, we should search for methods to be independent from intensity in SAR image interpretation.

Segmentation of SAR images is a fundamental process in SAR image interpretation. Due to the existence of correlated speckles, the segmentation of SAR images is commonly expressed as a very complex work [5]. The purpose of SAR image segmentation is to partition an image into areas of different characteristics [6]. It is a crucial point of SAR images interpretation in a way that the SAR image is decomposed in a mosaic of uniform areas. Recently, a number of methods have been proposed for SAR image segmentation including global segmentation techniques [7], [8], fuzzy clustering methods [9], spectral clustering algorithms [6], [10]-[13], and active contour model and level set [2], [5].

A global segmentation approach adapted to Gamma pdf of SAR images is used in [7] for SAR image segmentation. This parametric scheme is based on a polygonal grid model with a suppositional unknown number of regions. In this approach, the number of regions of the partition is estimated by minimizing the stochastic complexity. However, when the gray values of SAR images are not correctly described by Gamma pdf, like in textured speckle images, this technique will be failed. Furthermore, since a parametric noise model of the segmentation technique is considered, the parameters of regions need to be tuned, especially when the data differ from Gamma pdf such as in textured areas. So, this parametric technique only describes a unique class of textured data which can lead to analogous limitations to those obtained with the Gamma pdf.

In [8], the same Gamma distributed-based method as that in [7] was applied with different noise models. Compared with segmentation algorithm proposed in [7], this approach has some obvious advantages. It is based on a polygonal grid which can have an arbitrary topology and whose number of regions and regularity of its boundaries are obtained by minimizing the stochastic complexity of a quantified version on Q levels of the image [8]. Unlike in [7], this approach leads to a criterion without parameters that need to be tuned by the user. However, the appropriate value of Q, which minimizes the number of misclassified pixels (NMP), could not be estimated automatically in that approach. Moreover, if a texture area of an SAR image has other characteristics of parametric noise models such as Gaussian or Poisson, this technique may fail due to the nonlinear intensity inhomogeneity phenomenon mentioned above.

Recently, different forms of spectral clustering (SC) algorithms [6], [10]–[13] were proposed. Compared with traditional clustering algorithms, SC has some obvious advantages. It can recognize the clusters of unusual shapes and obtain the globally optimal solutions in a relaxed continuous domain by eigen decomposition [6]. However, the complexity of calculations exists in these methods and they are computationally expensive because of using an affinity matrix established by the likeness of each pair of pixels. So, the method needs to compute the eigenvectors of the affinity matrix. Furthermore, SC requires assigning a parameter, namely, the scaling parameter σ in the Gaussian radial basis function (RBF). Appropriate assigning of σ is determinant to obtain good segmentation results in SC. Unfortunately, it is difficult to select the suitable σ value, and it is always set manually. The improper value of σ can deteriorate the capabilities because SC is highly sensitive to σ, and different values of σ may cause to extremely different results [6].

In [14] and [15], the techniques established upon the active contour model and level set are proposed for segmentation of SAR images. These techniques are typically based on optimizing an energy function depending on the whole image and they can overcome the disadvantages of SC models. However, because the corresponding energy function has a local minimum, these methods may result in an unexpected state. So, in some cases, the level set function in these techniques cannot converge to a confident interval.

However, recent SAR image segmentation models [5], [9] tend to rely on intensity homogeneity in each region as well as no intention for segmenting the special objects in SAR images. On the other hand, nonlinearity of intensity inhomogeneity often occurs in SAR images as discussed above. These two methods cannot address the nonlinear intensity inhomogeneity phenomenon. Moreover, these methods need an initial curve to be created by user.

In this paper, we propose a new energy function named kurtosis wavelet energy (KWE) in order to solve these mentioned problems. This energy function

is an extension of that in [2]. KWE energy function will be concluded by pursuing the higher order statistics (HOS) and fourth order normalized cumulant, named kurtosis, implemented by wavelet and level sets. This energy function is used as a texture feature in this paper for SAR image segmentation application and has the following advantages: 1) it extracts more statistical characteristics of a specific region from an SAR image because the KWE energy formulation derived in this paper is one order greater of cumulant than the energy function proposed in [2], and 2) it does not need to have an initial contour, which should be initialized by a user. So, our algorithm can automatically perform the segmentation procedure of SAR images.

A new region-based active contour model for automatic segmentation of SAR images is proposed in this approach. We first define the kurtosis wavelet energy (KWE) function where it locally measures the region textures along the contour and texture features on two sides of the contour. So the texture of each region, can be characterized by using the energy of wavelet coefficients of each region in each sub-band of the decomposition process. The obtained texture is then formed into level set functions with a fourth order normalized cumulant term. Then, the regions and their interfaces can be modeled with these level set functions and a functional formulation can be calculated on these level sets in terms of fourth order normalized cumulant. Finally, the optimal automatic segmentation based method will be defined on textures by minimizing of this functional formulation.

Recently, Gabor filters are used to extract texture features for segmentation [16]-[18], but they have a major disadvantage, so that they produce a lot of redundancy and thus lots of feature channels. To overcome this problem, the structure tensor is employed to discriminate textures by many authors [19]-[23]. But the structure tensor misses so many other useful texture features that it is difficult to acquire perfect results [24].

In recent and thorough studies, Randen and Husøy [25], Haralik [26] and Haralik et al. [27] have reviewed and compared different approaches to texture feature extraction. Randen's images, which are fairly hard to classify even by eye, are becoming a benchmark for assessing different segmentation algorithms [28]-[31]. However, these techniques are not suitable for texture definition and discrimination of SAR images. The segmentation or classification methods by Randen *et al.* are not specifically designed for SAR images textures. In other words, the existence data as a ground truth for SAR images are different from Randen's data as a benchmark for optical texture algorithms.

Note that our method, termed as kurtosis wavelet energy model, is also related to SWE and LBF models which were presented in [2] and [32] respectively. In [32], the local intensity average values were derived as the minimizers of the energy function in a variational formulation. Whereas in this paper, a local texture of each region of a SAR image is derived as a minimizer of the proposed kurtosis wavelet energy function.

The remainder of this paper is organized as follows. In Section 2, we introduce kurtosis as an effective feature for SAR image segmentation. In section 3, derivation of classification formulation based on genetic algorithm is presented. The implementation and experimental results of our proposed algorithm on both simulated and real satellite SAR images are given in Section 4. Finally, Conclusions are drawn in Section 5.

Kurtosis Wavelet Energy Formulation as a Texture Feature

In probability theory and statistics, the moment generating function of a random variable X is defined by

$$M_X(\omega) = E_X\{e^{j\omega x}\} \tag{1}$$

The cumulant generating function of the same variable X is given by the logarithm of the moment generating function, $C_X(\omega)$ as

$$C_X(\omega) = \ln(M_X(\omega)) = \ln[E_X\{e^{j\omega X}\}] \tag{2}$$

After making a Taylor series expansion in the ω variable about the cumulant generating function, $C_X(\omega)$ which is given by equation (2), can obtain as below

$$C_X(\omega) = \ln[E_X\{e^{j\omega X}\}] = \sum_{n=1}^{\infty} k_n \frac{(j\omega)^n}{n!} \tag{3}$$

The coefficient of the Taylor series term ω^n, multiplied by $(-j)^n$, is called the nth-order cumulant of the random variable X and it is defined by

$$c_X^{(n)} = (-j)^n \frac{d^n}{d\omega^n} C_X(\omega)\Big|_{\omega=0} \quad \text{for} \quad n = 1,2,3,\ldots \tag{4}$$

The first order and the second order cumulants are the mean and the covariance of random variable X

respectively. It can be found by computing the first and the second order cumulants, $C^{(1)}{}_X(\omega)$ and $C^{(2)}{}_X(\omega)$, from equation (4) and rewriting them in terms of the moments. The first order moment is the mean and the second order moment is the covariance (or center of mass). These relations are defined by

$$\mu = c_x^{(1)} = m_x^{(1)} = E\{X\} \tag{5}$$

and

$$\text{cov.} = c_x^{(2)} = m_x^{(2)} - (m_x^{(1)})^2 = E\{X^2\} - (E\{X\})^2 \tag{6}$$

respectively.

It is reported [2] that whatever the order of cumulant as a feature for a SAR image increases, this feature will give the more statistical characteristics of a specific region from a SAR image. However, implementation of higher order cumulants will impose more calculations and time consuming. So, we should perform a trade off between the higher order and the complexity of calculations. In this paper, we propose to use the 4th-order normalized cumulant named kurtosis as a texture feature for segmentation of SAR images. We show that this selection gives the more statistical information of each region also it has logical computation and efficient implementation.

The expression yielding the fourth order cumulant of a random variable X from its moments can be derived by the relations that exist between moments and cumulants. The fourth order cumulant formulation of the interested variables is the following

$$\begin{aligned} c_X^{(4)} &= E\{(X-\mu)^4\} \\ &= m_X^{(4)} - 3[m_X^{(2)}]^2 - 4m_X^{(1)}.m_X^{(3)} \\ &\quad + 12[m_X^{(1)}]^2.m_X^{(2)} - 6[m_X^{(1)}]^4 \end{aligned} \tag{7}$$

In the above 4th order cumulant formulation, we can use it as a statistical feature for texture discrimination of different regions in SAR images. However, the formulation of 4th order cumulant derived in equation (7), is not inherently independent from the size of its random variable. On the other hand, in the SAR image segmentation approach, we should use a feature which it is invariant to image size. In particular, it is shown [33] that if a is an arbitrary scalar, then the cumulants of the random variables X and aX are related as

$$Y = aX \quad \Leftrightarrow \quad c_Y^{(m)} = a^m c_X^{(m)} \tag{8}$$

In order to make the 4th order cumulant formulation independent from its random variable, we provide a normalization of it. For this purpose, we consider the normalized cumulant of order *(m,n)* associated with random variable X as defined by

$$C_X^{(m,n)} = \frac{c_X^{(m)}}{\left|c_X^{(n)}\right|^{m/n}} \tag{9}$$

In the above equation, $C_X^{(m,n)}$ is considered as the m th-order cumulant normalized with n th-order cumulant. Such formulation can solve the image size variant problem and will act as image size invariant. Using this definition of cumulant for texture discrimination, it directly acts according to that this feature (normalized cumulant) is scalar invariant. This means that $C_{aX}^{(m,n)} = C_X^{(m,n)}$ for any nonzero scalar, a.

Typically, the order parameters m and n are selected as integer numbers in a way that $m>n$. Note that in this equation, the denominator $c_X^{(n)}$ should not be zero. So, we select $n=2$ to provide a logical choice, since $c_X^{(2)}$ is covariance and it is always nonzero for any random variable. If we select $m=4$ and $n=2$ and rewrite the normalized cumulant formulation derived in (9), we achieve the kurtosis formulation which we propose in this paper as [1]

$$\text{kurtosis}(X) = \frac{E\{(X-\mu)^4\}}{\sigma^4} = \frac{C_X^{(4)}}{(\text{var})^2} \tag{10}$$

where, μ is the mean of random variable X, *var* is the variance σ^2 of random variable X and it is a nonzero parameter (*var > 0*), and *E{t}* represents the expected value of the quantity t.

In equation (10), $C_X^{(4,2)}$ is named *kurtosis* which is the fourth order cumulant normalized with covariance. The *kurtosis* cumulant indicates the poignancy of the PDF histogram of a SAR image. In other words, this feature is the slope decrease curve of the PDF histogram of a SAR image. With a view to statistical calculations, kurtosis is a measure of how outlier-prone a distribution is. The kurtosis of the normal distribution is 3. Distributions that are more outlier-prone than the normal distribution have kurtosis greater than 3, and distributions that are less outlier-prone have kurtosis less than 3.

We use the kurtosis as a parameter of the Energy distribution of the wavelet coefficients in each sub-band of a SAR image.

Derivation of classification Formulation based on genetic algorithm

As we know, moments with higher orders can characterize textures in images. Since cumulants are able to give more statistical information, we can use high order cumulants to describe a texture of each region in SAR images. Thus, a texture discrimination of each region in SAR images can be done by the kurtosis explained in previous section.

We consider that a texture of each region in a SAR image is characterized by the kurtosis energy of its wavelet coefficients. Let $T_0(x,y)$ be a texture function of each region of a SAR image as below [1]

$$T_0(x,y) = \frac{\sum_m \sum_n W_\phi(j_0,m,n)\phi_{j_0,m,n}(x,y)}{\sqrt{MN}} + \frac{\sum_{i=H,V,D} \sum_{j=-j_0}^{-1} \sum_m \sum_n W_\psi^i(j,m,n)\psi^i_{j,m,n}(x,y)}{\sqrt{MN}} \quad (11)$$

where ψ is the wavelet function, ϕ is the scaling function and j_0 is the order of the decomposition. So, the energy of the wavelet coefficients in each sub-band can be obtained by the following sequence

$$\left(\left|W_\phi(j_0,m,n)\right|^2, \left|W_\psi^i(j,m,n)\right|^2, m,n \in Z, -j_0 \le j \le 1\right) \quad (12)$$

Aujol *et al.* [34] developed this model and showed experimentally that the distribution of the energy of the wavelet packet coefficients in a sub-band of any image follows a picky Gaussian form as below [1]

$$p_{X^2}(y) = \frac{A}{2\sqrt{y}} \exp\left(-\left(\frac{\sqrt{y}}{\xi}\right)^\eta\right) \quad \|y \ge 0 \quad (13)$$

where the parameters η and ζ were defined to classify the textured images. Such model can not classify regions of SAR images. In equation (13), η and ζ were computed from the first and second order moments of the energy distribution in each sub-band. Such definition is not good for our SAR image segmentation problem because of the instability that exists in the curve of moments. In our segmentation approach, η and ζ are the segmentation parameters and we are now in position to calculate these segmentation parameters in relation to the higher order moments (third and fourth order moments) of the energy distribution of the wavelet coefficients in each sub-band.

Suppose that for a given point p□r, where r is a desired region of a SAR image, the kurtosis wavelet Energy function F_p^{KWE} is followed by the distribution form of the kurtosis energy of the wavelet coefficients in a sub-band of each region. From equations (7) and (10), we have [1]

$$\begin{aligned} \text{Kurtosis} &= \frac{C^{(4)}_{|W_\varphi|^2}}{(C^{(2)}_{|W_\varphi|^2})^{4/2}} \\ &= \frac{m_X^{(4)} - 3[m_X^{(2)}]^2 - 4m_X^{(1)}.m_X^{(3)}}{(C^{(2)}_{|W_\varphi|^2})^{4/2}} \\ &\quad + \frac{12[m_X^{(1)}]^2.m_X^{(2)} - 6[m_X^{(1)}]^4}{(C^{(2)}_{|W_\varphi|^2})^{4/2}} \end{aligned} \quad (14)$$

The Gamma function $\Gamma(t)$ on R^+ is defined as

$$\Gamma(t) = \int_0^\infty e^{-u} u^{t-1} du \quad (15)$$

We assume that $p_{X^2}(y)$ defined in equation (13), is a probability density function of a sub-band of each region. Also, $|W_\varphi|^2$ is used instead of the random variable X^2. $|W_\varphi|^2$ is a symbol to show the energy of wavelet coefficients in each sub-band. So, we have

$$\int_0^\infty p_{|W\phi|^2}(W_\phi) dW_\phi = N \quad (16)$$

where N is the total number of pixels of the given detail SAR image. The value of parameter A in equation (13), can be obtained by using the equations (13), (15) and (16), and making the change of variable $(\frac{W_\varphi}{\xi})^\eta = u$ as below

$$A = \frac{N\eta}{\xi \Gamma(\frac{1}{\eta})} \quad (17)$$

Now, we can calculate the formulations of the first, second, third and fourth order moments of wavelet coefficients energy in terms of $\Gamma(t)$ from equations

$$\begin{aligned} m^{(1)}_{|W\phi|^2} &= E\{|W_\phi|^2\} = \int_{-\infty}^{+\infty} |W_\phi|^2 \, p_{|W\phi|^2}(|W_\phi|) d(|W_\phi|) \\ &= \int_0^{+\infty} (W_\phi)^2 . A \exp\left(-\left(\frac{W_\phi}{\xi}\right)^\eta\right) d(W_\phi) \quad (18) \\ &= \frac{A\xi^3}{\eta} . \Gamma\left(\frac{3}{\eta}\right), \end{aligned}$$

$$m^{(2)}_{|W\varphi|^2} = E\{|W_\varphi|^4\} = \frac{A\xi^5}{\eta} . \Gamma\left(\frac{5}{\eta}\right), \quad (19)$$

$$m^{(3)}_{|W\varphi|^2} = E\{|W_\varphi|^6\} = \frac{A\xi^7}{\eta}.\Gamma(\frac{7}{\eta}), \quad (20)$$

and

$$m^{(4)}_{|W\varphi|^2} = E\{|W_\varphi|^8\} = \frac{A\xi^9}{\eta}.\Gamma(\frac{9}{\eta}) \quad (21)$$

respectively.

Dividing (21) by (20), we obtain

$$\xi = \sqrt{\frac{m^{(4)}_{|W_\varphi|^2}}{m^{(3)}_{|W_\varphi|^2}} \frac{\Gamma(\frac{7}{\eta})}{\Gamma(\frac{9}{\eta})}} \quad (22)$$

Also, η can be obtained by rewriting equation (14) as below

$$\eta = F^{-1}(\text{Kurtosis}) = F^{-1}\left(\frac{C^{(4)}_{|W_\varphi|^2}}{(m^{(2)}_{|W_\varphi|^2})^{3/2}} \right) \quad (23)$$

where $F(x)$ is the function obtained by rewriting the kurtosis formulation in equation (14) in terms of the first, second, third and fourth order moments equations derived in equations (18)-(21) as follow [1]

$$F(x) = \frac{\Gamma^3(\frac{1}{\eta})\Gamma(\frac{9}{\eta}) - 3.N.\Gamma^2(\frac{1}{\eta}).\Gamma^2(\frac{5}{\eta}) - 4.N.\Gamma^2(\frac{1}{\eta}).\Gamma(\frac{3}{\eta}).\Gamma(\frac{7}{\eta})}{N.(\Gamma(\frac{1}{\eta}).\Gamma(\frac{5}{\eta}) - N\Gamma^2(\frac{3}{\eta}))^2} + \frac{12.N^2.\Gamma(\frac{1}{\eta})\Gamma^2(\frac{3}{\eta}).\Gamma(\frac{5}{\eta}) - 6.N^3.\Gamma^4(\frac{3}{\eta})}{N.(\Gamma(\frac{1}{\eta}).\Gamma(\frac{5}{\eta}) - N\Gamma^2(\frac{3}{\eta}))^2} \quad (24)$$

The graph of $F^{-1}(Kurtosis)$ is shown and compared with the other proposed methods in Fig. 2 [1].

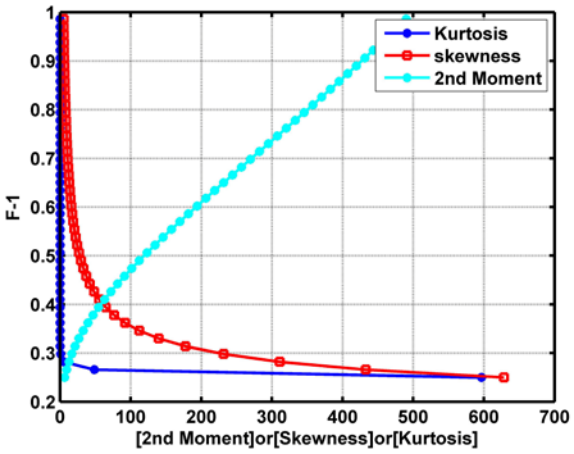

FIG. 2 THE CURVE OF F $^{-1}$ (KURTOSIS), F $^{-1}$ (SKEWNESS) AND F $^{-1}$ (2ND MOMENT) [1]

As depicted in Fig. 2, the curve of $F^{-1}(Kurtosis)$ is more stable than the $F^{-1}(skewness)$ and $F^{-1}(2^{nd}\ Moment)$ which were proposed in [2] and [34] respectively [35]. So, kurtosis is a good texture feature for satellite SAR image recognition. Now, we want to use the kurtosis values of the energy of wavelet coefficients of each texture in SAR images as a unique property to form a feature vector in the next section. In order to do that, we should study the active contour models.

Active contour models were first formulated by Mumford and Shah for the image segmentation problem [36]. Their function is practically difficult to be minimized because of the unknown contour and the no convexity of the function. Afterwards, Vese and Chan [37] optimized the active contour of the Mumford-Shah problem for a special case where the image is considered as a piecewise constant function. Their model does not contain any local intensity information. Then, Chunming Li *et al.* [32] proposed the LBF model to optimize the Vese-Cahn model. However, their model does not contain any statistical information, which is crucial for segmentation of SAR images with nonlinear intensity inhomogeneity. In this section, we introduce the level set based kurtosis model instead of the LBF model.

In [35], we defined a segmentation problem based on any textural region in SAR images. In that work, we defined the region $Re_k = \{p \in r \mid p \text{ belongs to the region } k\}$ where r was an open subset of R^2, K was the number of segmented regions (number of r_k), k was a parameter that shows the region index, p was a point of region, R_{kl} was the interface between region r_k and region r_l and the image was a function considered as $I: r \rightarrow R$. Also, we denoted that for all $k = 1,\ldots, K$, Re_k is an open set r_k given by a Lipschitz function $\Phi_k : r \rightarrow R$ so that $\Phi_k(p) > 0$ if pixel p is inside the region, $\Phi_k(p) = 0$ if pixel p lies in the border of the region, and otherwise $\Phi_k(p) < 0$, where Φ_k is the signed distance function to the region R_k. We can also determine r_k using the sign of Φ_k and the Heaviside distribution function H [1].

We define the following functional

$$T_{KWE-GA}(\Phi_i) = \varepsilon^p_{KWE-GA}(\Phi_i) + \mu\rho(\Phi) \quad (25)$$

where μ is a positive constant, $\varepsilon^{p}_{KWE\text{-}GA}$ is the kurtosis wavelet energy based on GA, and $\rho(\Phi)$ is the deviation of the level set function Φ from a signed distance function as below

$$\rho(\Phi) = \int_{r} \frac{1}{2}(|\nabla\Phi(p)| - 1)^2 \, dp \qquad (26)$$

We propose the kurtosis of the wavelet coefficients energy based on GA to be used as contour energy $\varepsilon^{p}_{KWE\text{-}GA}$ in (25).

We consider that for a given point $p \in r$, the kurtosis wavelet energy $\varepsilon^{p}_{KWE\text{-}GA}$ is followed by the distribution form of the kurtosis energy of the wavelet coefficients in a sub-band of each region.

To find the boundary of regions in SAR images, we

should minimize the integral of $\varepsilon^{p}_{KWE\text{-}GA}$ over all center points p in the all regions of a SAR image. So, we define the energy functional $\varepsilon(C,k_1,k_2)$ as bellow:

$$\varepsilon(C, k_1(p), k_2(p)) = \int_{r} \varepsilon^{p}_{KWE-GA}(C, k_1(p), k_2(p))dp \qquad (27)$$

The values of the functions $k_1(p)$ and $k_2(p)$ that minimize the KWE energy $\varepsilon^{p}_{KWE\text{-}GA}(C, k_1, k_2)$ are functions of the center point p of the kernel function $K(p-q)$. Thus, we claim that KWE energy $\varepsilon^{p}_{KWE\text{-}GA}$ has the localization property.

If we represent the contour $C \subset r$ with the level set of a Lipschitz function $\Phi: r \rightarrow R$, we get

$$\begin{aligned}\varepsilon_{KWE-GA}(\Phi, k_1, k_2) &= \int_{r} \varepsilon^{p}_{KWE-GA}(\Phi, k_1(p), k_2(p))dp \\ &= \gamma_1 \int [\int K_{|W_\phi|^2}(p-q)\,|\,I(q) - k_1(p)\,|^2 \, H(\Phi(p))dq]dp \\ &+ \gamma_2 \int [\int K_{|W_\phi|^2}(p-q)\,|\,I(q) - k_2(p)\,|^2 \, (1 - H(\Phi(p)))dq]dp\end{aligned} \qquad (28)$$

where H is the Heaviside function, and γ_1 and γ_2 are two constants.

Now, we define the new entire kurtosis wavelet energy based on GA function F_{KWE-GA} as

$$F_{KWE-GA}(\Phi, k_1, k_2) = \varepsilon_{KWE-GA}(\Phi, k_1, k_2) + \mu\rho(\Phi) \qquad (29)$$

where μ is a nonnegative constant, and $\rho(\Phi)$ is given by equation (26).

Keeping $k_1(p)$ and $k_2(p)$ fixed, and minimizing the $F_{KWE-GA}(\Phi, k_1, k_2)$, the active contour model proposed in this paper, is derived by equation (30)

$$\begin{aligned}\frac{\partial\Phi}{\partial t} &= -\delta_p(\Phi)(\gamma_1 e_1 - \gamma_2 e_2) + \nu\delta_p(\Phi)\mathrm{div}\left(\frac{\nabla\Phi}{|\nabla\Phi|}\right) \\ &+ \mu\left(\nabla^2\Phi - \mathrm{div}\left(\frac{\nabla\Phi}{|\nabla\Phi|}\right)\right)\end{aligned} \qquad (30)$$

where the functions e_1 and e_2 are computed by

$$e_1(p) = \int_{r} K_{|W_\phi|^2}(q-p)\,|\,I(p) - k_1(q)\,|^2 \, dq \qquad (31)$$

and

$$e_2(p) = \int_{r} K_{|W_\phi|^2}(q-p)\,|\,I(p) - k_2(q)\,|^2 \, dq \qquad (32)$$

respectively, and $k_1(q)$ and $k_2(q)$ are given by

$$k_1(q) = \frac{K_{|W_\varphi|^2}(q) * [H_p(\Phi(q))I(q)]}{K_{|W_\varphi|^2}(q) * H_p(\Phi(q))} \qquad (33)$$

and

$$k_2(q) = \frac{K_{|W_\varphi|^2}(q) * [(1 - H_p(\Phi(q)))I(q)]}{K_{|W_\varphi|^2}(q) * [1 - H_p(\Phi(q))]} \qquad (34)$$

Respectively [1].

Implementation and Test Results

To verify the satellite SAR image intensity model and the recognition method we proposed, the results of different algorithms on simulated and real SAR images will be presented in this section.

Segmentation of Simulated SAR Image

In this subsection, we first show one typical example of our large number of experiments with synthetic images and define the measures we adopted for performance analysis. We first simulate a 1-look case by the synthetic image of Fig. 3. It consists of four regions, as visual inspection can quickly indicate. It has been obtained by multiplying a perfect reflectivity synthetic image by a white exponential speckle noise [15]. The corresponding 1-look noisy image, as shown in Fig. 3(a), is generated by multiplying a realization of speckle. The ground truth image, as shown in Fig. 3(b), is used to calculate the error rates of the segmentations obtained by different algorithms.

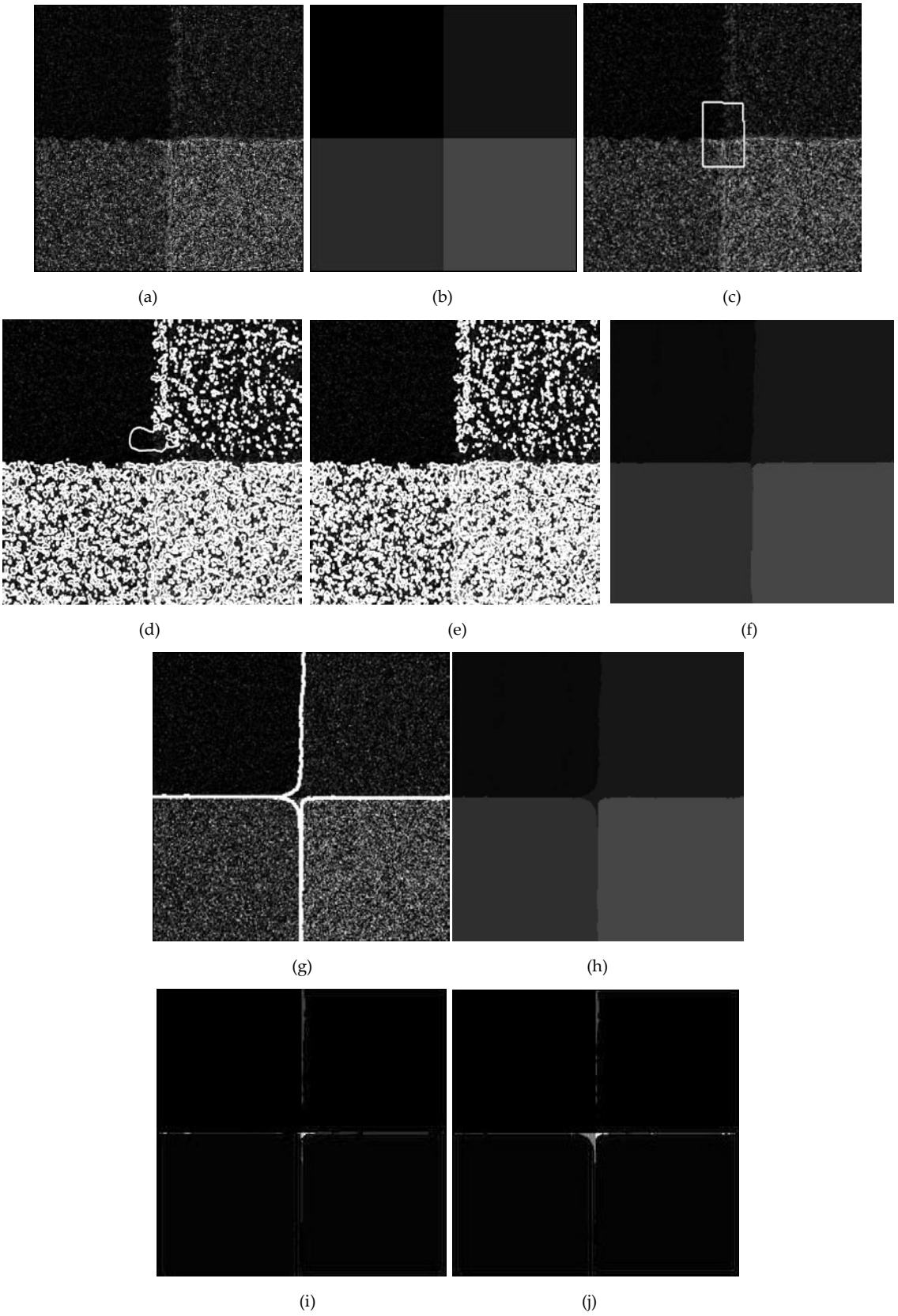

FIG. 3 (A) ONE-LOOK SIMULATED SAR IMAGE (222 × 222), (B) GROUND TRUTH, (C) INITIAL CURVE, (D) INTERMEDIATE CURVES PRODUCED BY KWE-GA METHOD PROPOSED IN THIS PAPER, (E) FINAL POSITIONS, (F) COMPUTED CLASSIFICATION KWE-GA METHOD PROPOSED IN THIS PAPER, (G) FINAL CONTOUR EXTRACTED BY THE METHOD PROPOSED IN [15], (H) SEGMENTATION OBTAINED BY THE METHOD PROPOSED IN [15], (I) THE DIFFERENCE BETWEEN THE RESULT OF KWE-GA AND GROUND TRUTH (ERROR RATE: 0.217%; THE NUMBER OF MISCLASSIFIED PIXELS: 107), AND (J) THE DIFFERENCE BETWEEN THE RESULT OF THE METHOD PROPOSED IN [15] AND GROUND TRUTH (ERROR RATE: 0.942%; THE NUMBER OF MISCLASSIFIED PIXELS: 464)

Fig. 3(c) shows the initial position of the evolving curve, Fig. 3(d) shows an intermediate position of the curves, Fig. 3(e) shows final position, and, finally, Fig. 3(f) displays the segmented and classified regions represented by their KWE value at convergence and GA to classify. The segmentation results by the method proposed in [15] are also shown in Fig. 3 and some comparisons between these two methods are reported. Fig. 3(g) shows the final contour convergence to segment the four regions with the method proposed in [15], and Fig. 3(h) shows the segmentation result obtained by this method. In comparison between Fig. 3(f) and 3(h), it can be visually found that KWE-GA method is better than the method proposed in [15]. Since we have the ground truth, we can also give objective evaluation in addition to visual inspection. The misclassified pixels and the error rate are computed by matching the classification result with the ground truth to evaluate the method. Fig. 3(i) shows the difference between Fig. 3(f) and 3(b) which is matching the KWE-GA result with the ground truth. Misclassified pixels are the pixels with non zero values in Fig. 3(i). The number of misclassified pixels can be estimated by counting the pixels with non zero values in Fig. 3(i). The number of misclassified pixels is 107. Since total number of pixels in Fig. 3(i) is $222 \times 222=49284$, we can compute the error from 107/49284=0.00217. So, the error rate for the KWE-GA method is 0.217%. Finally, Fig. 3(j) shows the difference between Fig. 3(h) and 3(b) which is matching the method proposed in [15] with the ground truth. The number of misclassified pixels and the error rate will be computed equal to 464 and 0.942% respectively from this Fig. From these reports, we found that the overall error rate is reduced about 0.725% by using KWE-GA method proposed in this paper. Therefore, the KWE-GA algorithm has the best classification result according to the error rate.

Segmentation of Real SAR Images

In this section, to demonstrate the applicability of the KWE-GA algorithm to real SAR image classification, experiments on a real SAR image are performed. To elucidate relative advantages of the KWE-GA algorithm with respect to KWE single method proposed in [35], the results of different algorithms on a genuine monolook satellite SAR image are presented. Not that when we deal with real SAR images classification, the ground truth corresponding to the SAR images being classified is absent generally. In this case, the evaluation of the classification result is based on visual inspection of the classified images.

The SAR image, as shown in Fig. 4(a), is a real single band SAR image acquired in August 1989 over the agricultural region of Feltwell (U.K.) by a fully polarimetric PLC-band NASA/JPL airborne sensor. More precisely, all three polarizations (HH, HV, and VV) acquired at band C, the HV and VV polarizations acquired at band L, and the HH polarization acquired at band P were used. The remaining channels (i.e., L-HH, P-HV, and P-VV) were discarded, because their histograms exhibit strong irregularities (for further details on this data set, we refer the reader to [38]-[40]). Hereafter, the adopted Feltwell bands will be synthetically denoted by "Feltwell-CHH," "Feltwell-CHV," …, "Feltwell-PHH."

To calculate the functions $k_1(q)$ and $k_2(q)$ given by equations (33) and (34) respectively, we should compute the kernel function $K_{|W_\varphi|^2}(p)$. For this reason, we first compute the value of $m^{(1)}_{|W_\varphi|^2}$, $m^{(2)}_{|W_\varphi|^2}$, $m^{(3)}_{|W_\varphi|^2}$ and $m^{(4)}_{|W_\varphi|^2}$ accordingly. To compute the first, second, third and fourth order moments of the energy distribution of the wavelet coefficients, we use wavelet decompositions of the maximum level L. Then, we calculate the kurtosis of these coefficients. We have tested several kinds of mother wavelets and several wavelet coefficients W^A_φ, W^H_φ, W^V_φ and W^D_φ. W^H_φ indicates that wavelet coefficients are measured along columns (horizontal direction), W^V_φ along rows (vertical direction), and W^D_φ along diagonals. W^H_φ, W^V_φ and W^D_φ are detail coefficients and W^A_φ contains approximation coefficients. We have selected to use the Haar mother wavelet as well.

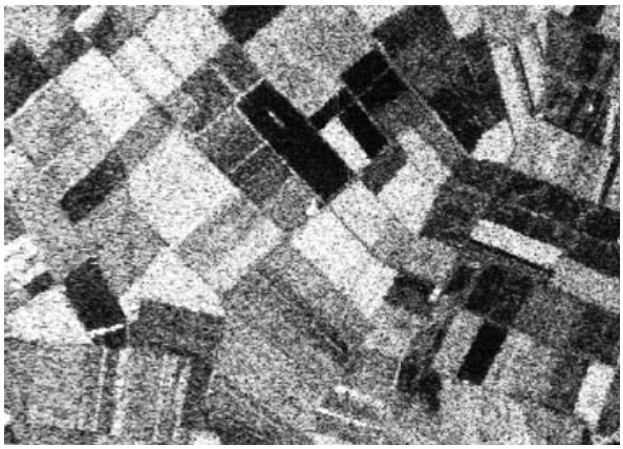

(a)

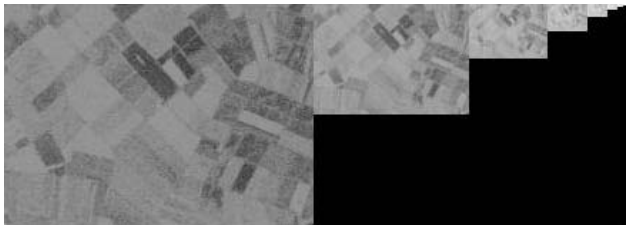

(b)

FIG. 4 (A) "FELTWELL-LHV" SAR IMAGE OF U.K. (309 × 433), (B) REPRESENTATION OF THE APPROXIMATION WAVELET COEFFICIENTS ENERGY $|W_{\varphi}^{A}|^2$ FROM LEVEL *1* TO *8* OF THE "FELTWELL-LHV" SAR IMAGE

After calculating the kurtosis of wavelet coefficients energy, the value of η can be computed from the curve of $F^{-1}(kurtosis)$ represented in Fig. 2, and then the value of ζ can be obtained from equation (22).

In Fig. 4(b), we show the approximation wavelet coefficients energy $|W_{\varphi}^{A}|^2$ based on genetic algorithm from level *1* to *8* of the "Feltwell-LHV" SAR image.

The value of the kurtosis of the approximation wavelet coefficients energy based on genetic algorithm represented in Fig. 4(b) is 1.087×10^{11}. It is obtained by equation (14). Now, we can get $\eta=0.2837$ from Fig. 5. This Fig. is the extended curve of Fig. 2 in the range $[0, 7 \times 10^{11}]$ of only the kurtosis-GA axis in detail.

Also, we calculated $\zeta = 0.2932$ and $A=3.7896 \times 10^{4}$ from equations (22) and (17), respectively. Note that the kurtosis parameters, η, ζ, and A are different for each SAR image.

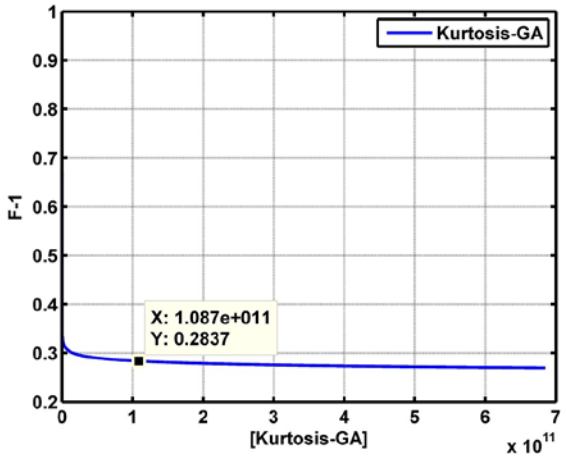

FIG. 5 THE CURVE OF *H* IN TERMS OF KURTOSIS OF FIG. 4(B)

To implement our KWE-GA texture recognition algorithm, the parameters in the experimentation are supposed as follows: $\gamma_1=1.0$, $\gamma_2=1.0$, $\nu = 0.004 \times 255^2$, $c_0 = 2$ (constant value of step function used as initial contour), time step $\tau = 0.1$, $\mu = 1.0$, and center point $p=1.0$.

On SAR image as shown in Fig. 4(a) which is shown in Fig. 6(a) again, three algorithms are used for classifying analysis: 1) SWE model, 2) KWE active contour model, and 3) the proposed KWE-GA.

The segmentation obtained by the SWE model [2] is shown in Fig. 6(b). One can see that the water area (middle top) is incorrectly segmented. Furthermore, the boundary between the vegetation and the water is not correctly defined (for better evaluation see Fig. 6(e)). The segmentation obtained by KWE, as shown in Fig. 6(c), improves the uniformity in the water region. However, there is still mis-segmentation in the water region [see the magnified of a selected area in Fig. 6(f)]. KWE-GA gets the best classification result, as shown in Fig. 6(d). The classification obtained by KWE-GA, improves the uniformity in the water region, and a local region of the crop in the water [see zoomed image in Fig. 6(g)] is consistently identified as vegetation.

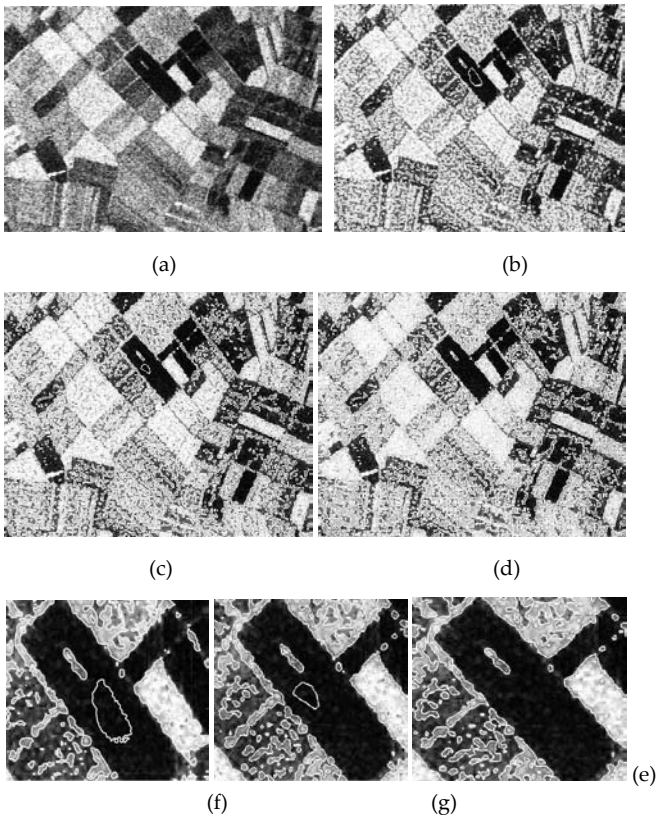

(a) (b) (c) (d) (e) (f) (g)

FIG. 6 (A) "FELTWELL-LHV" SAR IMAGE OF U.K. (309 × 433), (B) SEGMENTATION OBTAINED BY THE SWE, (C) SEGMENTATION OBTAINED BY KWE, (D) SEGMENTATION OBTAINED BY THE PROPOSED KWE-GA, (E) [RESPECTIVELY, (F) AND (G)] ZOOM OF AN AREA EXTRACTED FROM (B) [RESPECTIVELY, (C) AND (D)]

Conclusion

We have developed a new level set algorithm based on kurtosis value of wavelet coefficients energy as a feature extractor tools and genetic algorithm as a classifier tools for recognition of type of land cover of each region of satellite SAR images. A new energy named kurtosis wavelet energy (KWE) based on genetic algorithm (GA) is proposed to use as a recognition tools for texture classification of each region in the satellite SAR images. In comparison with the KWE single based segmentation model, the KWE based on GA achieves better performance on the SAR images. It also performs better than the method proposed in [15] in often cases. Experimental results show that the proposed KWE-GA algorithm is more robust for accurate recognition of several land cover kinds of satellite SAR images.

ACKNOWLEDGEMENT

The work described in this paper is supported by the Shahid Chamran University of Ahvaz (SCU) as a research proposal with code No. 901. The author would like to thank from the Shahid Chamran University of Ahvaz (SCU) for financial support.

REFERENCES

[1] G. Akbarizadeh, "A New Statistical-Based Kurtosis Wavelet Energy Feature for Texture Recognition of SAR Images," IEEE Transactions on Geoscience and Remote Sensing, Vol. 50, No. 11, November 2012, pp. 4358-4368.

[2] G. Akbarizadeh, "A New Kurtosis Wavelet Energy for Segmentation of SAR Images," 2nd National Conference on Soft Computing and Information Technology (NCSCIT), March 2012, pp. 1-4.

[3] M. Walessa and M. Datcu, "Model-Based Despeckling and Information Extraction from SAR Images," IEEE Transactions on Geoscience and Remote Sensing, Vol. 38, No. 5, Sep. 2000, pp. 2258-2269.

[4] L. R. Varshney, "Despeckling synthetic aperture radar imagery using the Contourlet Transform," Applications of signal processing, April 2004.

[5] Y. Shuai, H. Sun and G. Xu, "SAR Image Segmentation Based on Level Set With Stationary Global Minimum," IEEE Geoscience and Remote Sensing Letters, Vol. 5, No. 4, Oct. 2008, pp. 644-648.

[6] X. Zhang, L. Jiao, F. Liu, L. Bo and M. Gong, "Spectral Clustering Ensemble Applied to SAR Image Segmentation," IEEE Transactions on Geoscience and Remote Sensing, Vol. 46, No. 7, July 2008, pp. 2126-2136.

[7] F. Galland, N. Bertaux, and Ph. Réfrégier, "Minimum Description Length Synthetic Aperture Radar Image Segmentation," IEEE Transactions on Image Processing, Vol. 12, No. 9, Sep. 2003, pp. 995–1006.

[8] G. Delyon and Ph. Réfrégier, "SAR Image Segmentation by Stochastic Complexity Minimization With a Nonparametric Noise Model," IEEE Transactions on Geoscience and Remote Sensing, Vol. 44, No. 7, July 2006, pp. 1954–1961.

[9] P. R. Kersten, J.-S. Lee and T. L. Ainsworth, "Unsupervised Classification of Polarimetric Synthetic Aperture Radar Images Using Fuzzy Clustering and EM Clustering," IEEE Transactions on Geoscience and Remote Sensing, Vol. 43, No. 3, Mar. 2005, pp. 519–527.

[10] C. Fowlkes, S. Belongie, F. Chung and J. Malik, "Spectral Grouping Using the Nyström Method," IEEE Transactions on Pattern Analysis and Machine Intelligence, Vol. 26, No. 2, Feb. 2004, pp. 214–225.

[11] J. Shi and J. Malik, "Normalized Cuts and Image Segmentation," IEEE Transactions on Pattern Analysis and Machine Intelligence, Vol. 22, No. 8, Aug. 2000, pp. 888–905.

[12] S. X. Yu and J. Shi, "Multiclass Spectral Clustering," in Proceedings of the 9th IEEE International Conference on Computer Vision, Vol. 1, 2003, pp. 313–319.

[13] C. Ding, X. He, H. Zha, M. Gu and H. Simon, "A Min-max Cut Algorithm for Graph Partitioning and Data Clustering," in Proceedings of First IEEE International Conference on Data Mining (ICDM), 2001, pp. 107–114.

[14] I. B. Ayed, C. Vazquez, A. Mitiche and Z. Belhadj, "SAR Image Segmentation with Active Contours and Level Sets," In Proceedings of IEEE International Conference on Image Processing (ICIP), Vol. 4, 2004, pp. 2717–2720.

[15] I. B. Ayed, A. Mitiche and Z. Belhadj, "Multiregion Level-set Partitioning of Synthetic Aperture Radar Images," IEEE Transactions on Pattern Analysis and Machine Intelligence, Vol. 27, No. 5, May 2005, pp. 793–800.

[16] N. Paragios and R. Deriche, "Geodesic active regions and level set methods for supervised texture

segmentation," International Journal of Computer Vision, Vol. 46, No. 3, February 2002, pp. 223–247.

[17] B. Sandberg, T.F. Chan, and L. Vese, "A level-set and gabor-based active contour algorithm for segmenting textured images," UCLA Department of Mathematics, CAM report, July 2002, pp. 02–39.

[18] C. Sagiv, N.A. Sochen, and Y.Y. Zeevi, "Texture segmentation via a diffusion-segmentation scheme in the gabor feature space," Texture 2002, 2nd International Workshop on Texture Analysis and Synthesis, Vol. 18, No. 2, June 2002, pp. 123–128.

[19] R. de Luis-Garc´ıa, R. Deriche, and C. Alberola-L´opez, "Texture and color segmentation based on the combined use of the structure tensor and the image components," Signal Processing, Vol. 88, No. 4, April 2008, pp. 776–795.

[20] Y. Rathi, A. Tannenbaum, and O. Michailovich, "Segmenting images on the tensor manifold," in IEEE Conference on Computer Vision and Pattern Recognition, 2007, pp. 1–8.

[21] R. de Luis-Garcıa, R. Deriche, M. Rousson, and C. Alberola-Lopez, "Tensor processing for texture and colour segmentation," in Scandinavian Conference on Image Analysis. Springer, Vol. 2005, June 2005, pp. 1117–1127.

[22] Z. Wang and B.C. Vemuri, "Tensor field segmentation using region based active contour model," Lecture Notes in Computer Science, May 2004, pp. 304–315.

[23] M. Rousson, T. Brox, and R. Deriche, "Active unsupervised texture segmentation on a diffusion based feature space," in IEEE Computer Society Conference on Computer Vision and Pattern Recognition, Vol. 2, 2003, pp. 699–704.

[24] H. Lu, Y. Liu, Z. Sun and Y. Chen, "An active contours method based on intensity and reduced Gabor features for texture segmentation," 16th IEEE International Conference on Image Processing (ICIP), Nov. 2009, pp. 1369-1372.

[25] T. Randen and J. H. Husøy, "Filtering for texture classification: A comparative study," IEEE Transactions on Pattern Analysis and Machine Intelligence, Vol. 21, No. 4, April 1999, pp. 291-310.

[26] R. M. Haralick, "Statistical and structural approaches to texture," Proceedings of the IEEE, Vol. 67, No. 5, May 1979, pp. 786-804.

[27] R. M. Haralick, K. Shanmugam, and I. Dinstein, "Textural features for image classification," IEEE Transactions on Systems, Man and Cybernetics, Vol. smc-3, No. 6, Nov. 1973, pp. 610-621.

[28] C. C. Reyes-Aldasoro and A. Bhalerao, "The Bhattacharyya space for feature selection and its application to texture segmentation," Pattern Recognition, Vol. 39, No. 5, 2006, pp. 812-826.

[29] T. Ojala, K. Valkealahti, E. Oja, and M. Pietik, "Texture discrimination with multidimensional distributions of signed gray level differences," Pattern Recognition, Vol. 34, No. 3, 2001, pp. 727-739.

[30] N. Malpica, J. E. Ortu, and A. Santos, "A multichannel watershed-based algorithm for supervised texture segmentation," Pattern Recognition Letters, Vol. 24, No. 9, 2003, pp. 1545-1554.

[31] T. Ojala, M. Pietikainen, and T. Maenpaa, "Multiresolution gray-scale and rotation invariant texture classification with Local Binary Patterns," IEEE Transactions on Pattern Analysis and Machine Intelligence, Vol. 24, No. 7, July 2002, pp. 971-987.

[32] C. Li, C. Kao, J. Gore and Z. Ding, "Minimization of Region-Scalable Fitting Energy for Image Segmentation," IEEE Transactions on Image Processing, Vol. 17, No. 10, Oct. 2008, pp. 1940-1949.

[33] J. A. Cadzow, "Blind Deconvolution via Cumulant Extrema," IEEE Signal Processing Magazine, Vol. 13, No. 3, May 1996, pp. 24-42.

[34] J. F. Aujol, G. Aubert and L. B. Feraud, "Wavelet-based level set evolution for classification of textured images," IEEE Transactions on Image Processing, Vol. 12, No. 12, Dec. 2003, pp. 1634–1641.

[35] G. A. Rezai-Rad and G. Akbarizadeh, "A New Readout Circuit Structure for SAR Satellite Imaging Sensors," International Review of Electrical Engineering (IREE), Vol. 5, No. 1, pp. 281-290, February 2010.

[36] D. Mumford and J. Shah, "Optimal approximations by piecewise smooth functions and associated variational problems," Communications on Pure and Applied Mathematics, Vol. 42, No. 5, 1989, pp. 577–685.

[37] L. Vese and T. Chan, "A multiphase level set framework for image segmentation using the Mumford and Shah model," International Journal of Computer Vision, Vol. 50, No.3, Dec. 2002, pp. 271–293.

[38] G. Moser, J. Zerubia and B. Serpico, "SAR amplitude probability density function estimation based on a generalized gaussian model," IEEE transactions on image processing, vol. 15, No. 6, pp. 1429-1442, June 2006.

[39] G. Moser, J. Zerubia and B. Serpico, "Dictionary-based stochastic expectation–maximization for SAR amplitude probability density function estimation," IEEE transactions on geosience and remote sensing, vol. 44, No. 1, pp. 188-200, January 2006.

[40] G. Moser, and B. Serpico, "Generalized minimum-error thresholding for unsupervised change detection from SAR amplitude imagery," IEEE transactions on geosience and remote sensing, vol. 44, No. 10, pp. 2972-2982, October 2006.

Gholamreza Akbarizadeh was born on July 14, 1981, in Shiraz, Iran. He received the B.S. degree in Electrical and Electronics Engineering from the Khajeh-Nasir Tousi University of Technology (KNTU), Tehran, Iran, in 2003, the M.S. degree in Electrical and Electronics Engineering from the Iran University of Science and Technology (IUST), Tehran, Iran, in 2005 and the Ph.D. degree in Electrical and Electronics Engineering from the Iran University of Science and Technology (IUST), Narmak, Tehran, Iran, in 2011. Since 2003 to 2011, he has worked at DSP R&D research laboratory as a senior researcher. Dr. Akbarizadeh is an assistant professor and faculty member of Electrical Engineering Department at Shahid Chamran University of Ahvaz (SCU). He has more than twenty published papers in different international Electrical Engineering conferences and journals. He is member of some international scientific societies such as IEEE and also Iranian Machine Vision & Image Processing Society (MVIP). His research interests include Image Processing, Pattern Recognition, Machine Vision, and Remote Sensing Analysis.